Journal of Polymers and the Environment (2018) 26:3677–3697
https://doi.org/10.1007/s10924-018-1246-z

ORIGINAL PAPER

Removal of Congo Red from Aqueous Solution by Hydroxyapatite Nanoparticles Loaded on Zein as an Efficient and Green Adsorbent: Response Surface Methodology and Artificial Neural Network-Genetic Algorithm

Shima Ghanavati Nasab[1] · Abolfazl Semnani[1] · Abbas Teimouri[2] · Homa Kahkesh[2] · Tahereh Momeni Isfahani[3] · Saeed Habibollahi[2]

Published online: 12 May 2018

Abstract
This study is based on the application of hydroxyapatite nanoparticles loaded on Zein (Zein/nHAp) as an efficient adsorbent for the removal of Congo red from aqueous solutions. The properties of the adsorbent were characterized using various techniques including FT-IR, XRD, FE-SEM, and BET. The influence of five parameters such as pH, temperature, contact time, initial dye concentration, and adsorbent dosage on the removal percentage of the dye was investigated. The optimum conditions of 5.83, 34.32 °C, 5.20 min, 392.10 ppm, and 0.007 g were achieved for pH, temperature, contact time, initial dye concentration, and adsorbent dosage, respectively. The maximum removal percentage of 99.48% was obtained under the optimum condition that exhibited high adsorption potential of the used adsorbent. Central composite design (CCD) under response surface methodology and artificial neural network-genetic algorithm (ANN-GA) were utilized for optimization of parameters. Comparison of the results of the two models in terms of coefficient of determination (R^2) and mean absolute percentage error confirmed the prediction potential of CCD and ANN-GA. Higher ability and accuracy of ANN-GA in prediction was found based on given results. The experimental equilibrium data were studied by Langmuir, Freundlich, Temkin and Dubinin-Radushkevic isotherm models and explored that the data well presented by Langmuir model with maximum adsorption capacity of 416.66 mg/g. The adsorption kinetic was well-fitted by the pseudo-second-order model. The thermodynamics of the adsorption displayed spontaneous and endothermic nature of the process. Regeneration investigation showed that Zein/nHAp can impressively be reused, indicating that the adsorbent was a promising one for the removal of Congo red from aqueous solution.

✉ Abolfazl Semnani
a.semnani1341@gmail.com

[1] Department of Chemistry, Faculty of Sciences, University of Shahrekord, P. O. Box 115, Shahrekord, Iran

[2] Chemistry Department, Payame Noor University, Tehran 19395-3697, Iran

[3] Department of Chemistry, Islamic Azad University-Arak Branch, P. O. Box 38135-567, Arak, Iran

Graphical Abstract

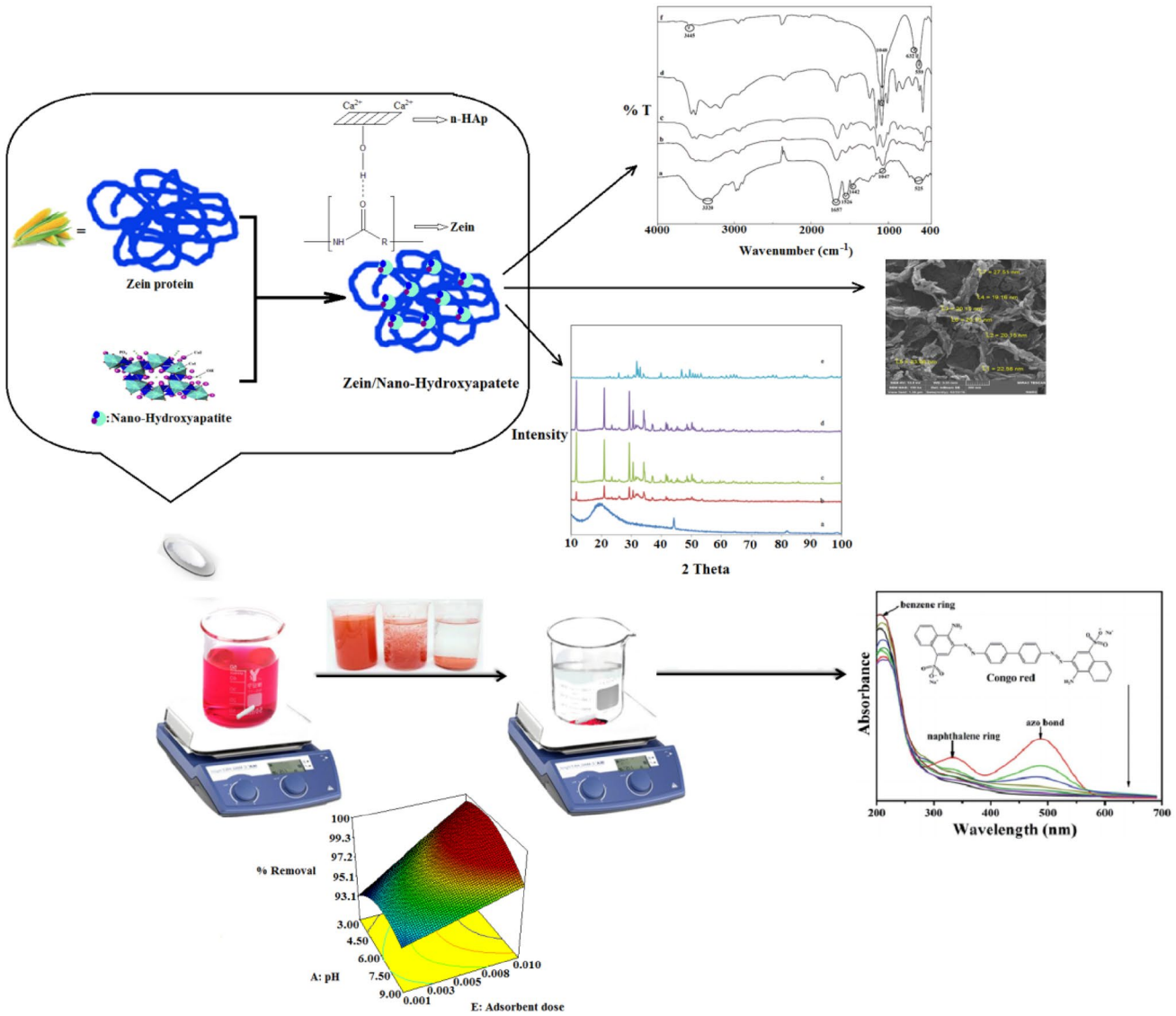

Keywords Adsorption · Congo red dye · Zein · Nanohydroxyapatite · Design of experiment · Artificial neural network-genetic algorithm

Introduction

Recently, water pollution has raised drastic concerns, because large amounts of water are evacuated into the environment. Therefore, removal of different contaminants from industrial effluents has got a judgmental subject [1]. Synthetic dyes, as main pollutants in industrial sewage, are vastly applied in textile, leather, tanning, paper, food processing, plastic, cosmetics, rubber, and printing. The dyes result in great dangers and toxicity to the human environment as well as severe health problems if they release into

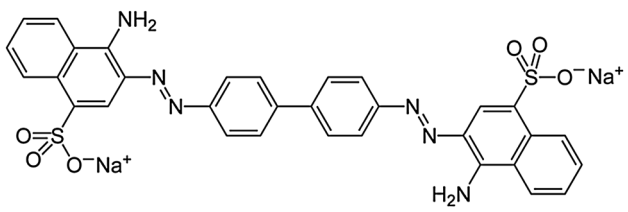

Fig. 1 Chemical structure of Congo red

the environment [2, 3] because they are steady, uncooperative, coloring agent, and even possibly carcinogenic and toxic [4].

Congo red (CR) named as the sodium salt of benzidinediazo-bi's-1-naphtylamine-4-sulfonic acid (Fig. 1) belongs to anionic dyes that cause health problems including difficulties in breathing, vomiting, diarrhea, and nausea. It is not biodegradable and easily metabolized to benzidine that is known human carcinogen. CR leads to the allergic reaction when it is exposed to organism. It looks to be a pretty toxic agent in terms of its resistance to heat, chemical reagent, and capability of producing cancer and mutagens owing to the existence of different reactive center and charge nature [5].

Removing dyes from aquatic solution has got a significant and stimulating issue in wastewater treatment [6]. A variety of techniques has been utilized for removal of dyes [7] such as adsorption [8–10], flocculation [11], oxidation [12], and electrolysis [13]. While among them the adsorption, as a better and superior candidate, has attracted more attention due to its high efficiency, ease of application, simplicity of design, vast fitness for different kinds of dyes and large-scale capacity, economy, low chemicals, and energy consumption, as well as no production of mud [14–16]. Green, non-toxic, and low-cost adsorbents benefit from a high surface area and reactive sites are desirable features for any adsorbents to eliminate large amounts of dyes in a short time in the recyclable process [17]. To date, different materials have been explored as the adsorbent for removal of hazardous contaminants such as activated carbon, graphene nanosheets, multi-walled carbon nanotubes, cedar sawdust, and crushed brick, magnetic Chitosan/graphene oxide composite, rice husk, and other reasonable cost adsorbents [1].

Zein, the prolamin from corn, is a heterogeneous combination of disulfide-linked polypeptides with 44 kDa molecular weight and includes 21–26% glutamic acid, 20% leucine, 10% proline, and 10% alanine. It has large availability and is not soluble in water only if alcohol exists, as well as is a top secondary product from bioethanol industry. Zein has been discovered to be biodegradable, biocompatible and has high adsorption capacity for removal of reactive dyes as an effective adsorbent [18].

Nowadays, the application of nanostructured adsorbents such as nanoscale zero-valent iron, carbon nanotubes, nanosized hydroxyapatite (nHAp), and nanocomposite have been expanded [19]. Because nanoparticles have a large surface area with a large number of empty reactive sites that provides high adsorption capacity and increases adsorption efficiency [20].

Nanosized hydroxyapatite [(HAp), $Ca_{10}(PO_4)_6(OH)_2$], a main inorganic constituent of the hard tissues (bones and teeth) in the human body, is biodegradable, biocompatible, and is not toxic. nHAp is able to make a bond with organic molecules. Hence it is employed to modify surface properties of many substrates [6, 21]. Anchoring nHAp with Zein to obtain Zein/nanohydroxyapatite, as an efficient adsorbent, can significantly enhance the removal percentage, adsorption capacity, and removal rate due to increase in surface area and a number of reactive sites.

Various methods are applied for process optimization. In order to obtain precise processes, choosing suitable techniques to model and optimize of variables is a critical stage. Experimental design methodologies and chemometric methods are helpful to optimize the impressive parameters with the lowest number of experiments [22]. Central composite design (CCD) under response surface methodology (RSM) and artificial neural network based on genetic algorithm (ANN-GA) are the most successful techniques for modeling and optimization studies. Because they enhance process efficiency, decrease the number of variables in the process by considering just the most important parameters, and also decrease operation cost and experimental time [23].

Response surface of methodology is a set of experimental design methods which employs statistical and mathematical techniques for modeling the experiments, rating the impact of some factors, and acquiring the optimum conditions for favorable response with a minimum number of planned experiments. RSM describes the relationship between several independent variables and one or more responses. The aim of RSM technique is to achieve the optimum response and discover how the response varies in a given direction by regulating the design variables [24].

The most famous artificial neural network (ANN) layout is accompanied with multi-layered perceptron consist of input, hidden and output layers and various number of neurons in each layer [24]. This method is able to tackle incomplete data and sort out nonlinear problems. ANN can accomplish predictions and generalizations at high speed, once trained. Nevertheless, it has some restrictions. For example, it is not possible to guarantee the smoothness of ANN models in optimizations phase. The optimization of ANN parameters can get better by applying genetic algorithm (GA), a stochastic global search algorithm, to get qualified performance. GA associated with ANN is an impressive means for prediction and optimization of any complex process parameters [25].

In continuation of our previous works in removal [26, 27], in the current project, Zein modified with nanohydroxyapatite as an efficient adsorbent was prepared and characterized by Field emission scanning electron microscopy (FE-SEM), Fourier transform infrared spectroscopy (FT-IR), X-ray diffraction (XRD), and BET. Afterward, it was used for the adsorption of Congo red dye from aqueous solution. The influence of some significant variables such as pH, temperature, contact time, initial dye concentration, and adsorbent dosage on the determination of CR was explored and optimized by central composite design (CCD) under response

surface methodology (RSM) and artificial neural network-genetic algorithm (ANN-GA). The coefficient of determination (R^2) and mean absolute percentage error (MAPE) of CCD and ANN-GA were compared. The kinetic, isotherm and thermodynamic parameters were computed to assess rate constants and adsorption mechanism. Applicability of the adsorbent in real samples and recyclability of Zein/nHAp were also studied.

Experimental

Materials and Instruments

Chemicals including Congo red (CR), Zein, $Ca(NO_3)_2{\cdot}4H_2O$, $(NH_4)_2HPO_4$, C_2H_6O and NH_4OH were purchased from Merck and Acros. The stock solution (500 ppm) of Congo red was obtained by dissolving of 50 mg CR in 100 ml double distilled water, then the appropriate dilution was done to achieve a working solution with desired concentration. The Zein/nHAp was synthesized and characterized by FTIR, XRD, FE-SEM, and BET. The morphology of the Zein/nHAp was studied by field emission scanning electron microscopy (FE-SEM; VEGA//TESCAN-LMU). X-ray diffraction (XRD) pattern was registered by an automated diffractometer with Cu K_α radiation (ASENWARE AW-XDM300, 40 KV). Fourier transform infrared spectroscopy of the adsorbent was recorded using FT-IR spectrophotometer (Model; FT-IR JASCO 680 plus). The BET analysis was done by BEL: PHS 1020. The achieved spectra were analyzed. The pH measurements were performed applying pH/Ion meter model-826 (Metrohm, Switzerland, Swiss) and the CR concentration was determined with UV-2401PC Research-Grade UV–Vis spectrophotometer at wavelength of 497 nm. The design expert software version 7.0.0 Trial was utilized for experimental design analysis and their subsequent regression analysis, also the Matlab R2014a software has been used for ANN and GA processes.

Preparation of Zein/nHAp

The Zein/nHAp composite was synthesized via a co-precipitation method. For the synthesis of Zein/nHAp with contents of 50 wt% of Zein, firstly, a solution of 2.94 g $Ca(NO_3)_2{\cdot}4H_2O$ in 50 ml water was dropwise poured to a solution of 0.986 g $(NH_4)_2HPO_4$ in 50 ml water. Subsequently, Zein solution, prepared by dissolving 1.25 g Zein in 15.8 ml ethanol, was added dropwise. The pH of the final solution was kept above 10 using 25% ammonia solution. Then, the solution was stirred for 4 h and maintained for 24 h at room temperature. The obtained Zein/nHAp was filtered from the reaction mixture and rinsed with distilled water until the pH of the filtrate was close to 7. Finally, Zein/nHAp was further rinsed with ethanol and dried at 70 °C for about 12 h. A series of Zein/nHAp composites with Zein contents of 30 and 70 wt% were synthesized too.

Adsorption Experiments

The adsorption of Congo red onto Zein/nHAp were carried out in batch experiments. According to the experimental design pattern, each run was repeated four times and after considered time in each run, Zein/nHAp was regathered by filtration and the concentration of CR in the supernatant was evaluated by UV–Vis spectrophotometer. The concentration of CR was calibrated by the Beer–Lambert law at the maximum wavelength. Removal percentage and equilibrium adsorption of the dye by Zein/nHAp from the aqueous solution were calculated applying the following relationships respectively [28].

$$\%\ \text{Removal} = \frac{C_0 - C_e}{C_0} \times 100 \tag{1}$$

$$q_e = \frac{C_0 - C_e}{W} \times V \tag{2}$$

where C_0 and C_e are the first and equilibrium concentrations of the dye in mg l^{-1}, respectively. The q_e is the adsorbed amount of dye at equilibrium (mg g^{-1}), V is the volume of the solution (in L) and w is the mass of Zein/nHAp (in g). The recyclability studies of the adsorbent for dye adsorption were performed by scattering the CR loaded Zein/nHAp (Zein/nHAp-CR) in ethanol solution. Then the adsorbent was washed with distilled water until the pH of the filtrate reached 7 and dried at 45 °C.

Experimental Design and Statistical Analysis

Response Surface Methodology (RSM) is a statistical method for optimization and studying the relevance between independent variables and response as linear and nonlinear form to assess an improved response. Central Composite Design (CCD) in RSM, as a widely applicable optimization model, utilized for fitting a second order model, particularly in the removal process [29]. In this study, five factors including pH, time, temperature, initial dye concentration and adsorbent dosage were considered in tests with five levels. The extents and levels of the five independent variables with actual and coded amounts of each parameter are revealed in Table 1. The independent variables are coded to two levels; low (−1) and high (+1), whereas the axial points are coded as −2 and +2. A five-level-five-factor ½ fraction central composite design was applied to suit a second-order response surface model demanded 32 experiments, consist of 26 factorial and axial points, and 6 replicates at the center points that are employed

Table 1 Experimental factors and levels in the central composite design

Factors	Unit	Symbol	Levels				
			$-\alpha$	Low (−1)	Central (0)	High (+1)	$+\alpha$
pH		X_1	3.0	4.5	6.0	7.5	9.0
Contact time	min	X_2	5.0	12.5	20	27.5	35.0
Temprature	°C	X_3	20.0	27.5	35.0	42.5	50.0
CR concentration	mg/l	X_4	40	130	220	310	400
Adsorbent dosage	g	X_5	0.001	0.00325	0.0055	0.00775	0.01

to assess the experimental error (pure error) and the reproducibility of the data. 32 experiments were managed in random order and the removal percentage was computed. The complete CCD design matrix in terms of the actual independent variable is offered and the related results are presented in Table 2. The experiments were conducted several times to diminish errors.

The linear and quadratic model with interactions is observed in the following equation [30].

$$y = \beta_0 + \sum_{i=1}^{k} \beta_i X_i + \sum_{i=1}^{k} \beta_{ii} X_i^2 + \sum_{i=1}^{k} \sum_{j=1}^{k} \beta_{ij} X_i X_j + \varepsilon \quad (3)$$

Table 2 Central composite design and the observed and predicted values for removal efficiency (%) of CR by Zein/nHAp nanocomposite

Run	Factors					Removal efficiency (%)		
	X_1	X_2	X_3	X_4	X_5	Experimental	Predicted	Residual
1	7.50	27.50	42.50	310.00	0.0077	98.00	98.00	0.00
2	4.50	27.50	27.50	310.00	0.0077	97.30	97.27	0.03
3	6.00	20.00	35.00	220.00	0.0055	96.50	96.60	0.10
4	6.00	5.00	35.00	220.00	0.0055	97.50	97.43	0.07
5	6.00	20.00	35.00	400.00	0.0055	99.00	99.07	0.07
6	6.00	35.00	35.00	220.00	0.0055	96.90	96.88	0.02
7	6.00	20.00	35.00	220.00	0.0010	96.80	96.75	0.05
8	4.50	12.50	42.50	130.00	0.0032	96.30	96.36	0.06
9	7.50	12.50	42.50	310.00	0.0032	96.80	96.81	0.01
10	7.50	12.50	27.50	310.00	0.0077	96.80	96.79	0.01
11	4.50	27.50	42.50	130.00	0.0077	95.20	95.25	0.05
12	4.50	12.50	27.50	310.00	0.0032	96.00	95.99	0.01
13	6.00	20.00	20.00	220.00	0.0055	96.30	96.29	0.01
14	3.00	20.00	35.00	220.00	0.0055	95.00	94.98	0.02
15	4.50	27.50	27.50	130.00	0.0032	96.50	96.53	0.03
16	7.50	27.50	27.50	310.00	0.0032	96.90	96.89	0.01
17	6.00	20.00	35.00	220.00	0.0055	96.54	96.60	0.07
18	7.50	12.50	27.50	130.00	0.0032	97.60	97.65	0.05
19	6.00	20.00	35.00	220.00	0.0055	96.60	96.60	0.00
20	6.00	20.00	35.00	220.00	0.0055	96.70	96.60	0.10
21	6.00	20.00	50.00	220.00	0.0055	96.80	96.72	0.08
22	6.00	20.00	35.00	40.00	0.0055	97.80	97.64	0.16
23	7.50	27.50	27.50	130.00	0.0077	94.60	94.64	0.04
24	4.50	12.50	42.50	310.00	0.0077	97.90	97.90	0.00
25	6.00	20.00	35.00	220.00	0.0055	96.50	96.60	0.10
26	6.00	20.00	35.00	220.00	0.0055	96.70	96.60	0.10
27	4.50	27.50	42.50	310.00	0.0032	97.20	97.19	0.01
28	6.00	20.00	35.00	220.00	0.0100	96.50	96.46	0.04
29	7.50	27.50	42.50	130.00	0.0032	97.20	97.26	0.06
30	4.50	12.50	27.50	130.00	0.0077	97.40	97.44	0.04
31	7.50	12.50	42.50	130.00	0.0077	96.10	96.17	0.07
32	9.00	20.00	35.00	220.00	0.0055	95.10	95.03	0.07

where y states response (removal percentage), X_i and X_j show independent variables, β_0 represents the intercept constant, β_i expresses the coefficients of linear terms, β_{ij} indicates the coefficient of quadratic terms, ε represents experimental error, and k expresses the number of independent variables. Analysis Of Variance (ANOVA), regression studies, and plotting of 3D plot were utilized to find the desired conditions for the response [31].

Artificial Neural Network-Genetic Algorithm

The neural network code of MATLAB (R2014a) software was selected to predict the removal percentage of the dye. A three layers ANN with a tangent sigmoid transfer function (tansig) at the hidden layer, a linear transfer function (pure line) at output layer and Levenberg–Marquardt backpropagation algorithm with 1000 iterations were used. The data were randomly divided into three groups (70% data for training set, 15% data for validation set and 15% data for a testing set). In this article, five neurons including pH, time, temperature, initial dye concentration and adsorbent dosage for the input, 9 neurons in the hidden layer, and one neuron (removal percentage) in the output layer were employed. All the data (input and output) for ANN models were standardized between 0.1 and 0.9 to keep away from numeric over fitting owing to pretty large or small weights. The used normalization equation is as follows [32, 33].

$$y = \left(\left(\frac{X_i - X_{min}}{X_{max} - X_{min}} \right) \times 0.8 \right) + 0.1 \quad (4)$$

where y is the normalized amount of X_i, the X_{max} and X_{min} are the most and least values of X_i, respectively. The measure for option of the optimum ANN structure is the mean square error (MSE) of the test data and the coefficient of assessment (R^2) that is explained as follows [34, 35].

$$MSE = \frac{1}{P} \sum_{P=1}^{P} (d_p - o_p)^2 \quad (5)$$

$$R^2 = 1 - \frac{\sum_{P=1}^{P} (d_p - O_p)^2}{\sum_{P=1}^{P} (O_P)^2} \quad (6)$$

where d_p and O_P are the desired and computed outputs, respectively. The evaluated results presented here are those that turn into the lowest point on the error.

Optimum Conditions Based on Genetic Algorithm

The genetic algorithm (GA) has been used as a successful technique for working out linear and nonlinear problems made by the process of natural selection and genetic evaluation. GA applies mutation, crossover, and opting operators to a population of encoded variable space. The algorithm investigation varies areas of the variable space and directs the search to the area where a high possibility of global optimum exists. More details about GA brought up elsewhere [17, 36]. In the suggested method, the genetic algorithm can be used after expanding the central composite design and trained ANN to optimize the input variables, with an objective to maximum the removal percentage of dye. GA based optimization on processes was executed by using CCD and the trained ANN model as the fitness functions to give the global optimized solutions.

Results and Discussion

Characterization of Adsorbent

Figure 2 compares the FT-IR characterization of pure Zein (a), pure nHAp (f), and Zein/nHAp composite with different Zein content including 70 wt% (b), 50 wt% (c), and 30 wt% (d). The spectrum of pure Zein, shown in Fig. 2a, has two bands at 1657 and 1526 cm^{-1} which indicate the stretching vibrations of C–O in amide groups I and II, respectively. The peak at 1271 cm^{-1} is attributed to bending vibrations of N–H. These peaks confirmed alpha helix secondary protein structure of Zein. 1657 cm^{-1} is related to the O–H vibrations, 1101 and 1047 cm^{-1} come from phosphate stretching vibrations. Peaks at 525, 825, 1442, and 1526 cm^{-1} stand for the presence of amino acids consist of cysteine, tyrosine, glutamine, and lysine, respectively [37, 38]. Also, the spectrum of pure nHAp illustrated in Fig. 2f, indicates that the bands at 632 and 3140 cm^{-1} are corresponded to the hydroxyl groups and the peaks at 560–610 cm^{-1} and 1000–1100 cm^{-1} are due to PO_4^{3-} stretching vibrations [39]. Compared to Zein, peaks at 970 and 1657 cm^{-1} appeared in the composite and corresponded to stretching vibrations of phosphate and hydroxyl vibrations [38]. Figure 2b–d also represents the intensity of distinctive bands of HAp in the spectrum of the composite is changeable and depends on the concentration of nHAp in the composite. The intensity of characteristic peaks of nHAp in composites with different wt% is in the order: b < c < d (shown in Fig. 2), respectively. Because the concentration of nHAp increased from b to d [40]. In addition, it can be seen characteristic bands of both nHAp and Zein such as the peaks corresponding to hydroxyl, amino, and amide groups exist in the spectra of Zein/nHAp, except for slight band shifts and peak height reduces possibly due to chemical reaction between Zein and nHAp. FT-IR analysis of adsorbent proved that nHAp introduced into Zein after modification.

FE-SEM presents helpful information about morphology and particle size of Zein/nHAp. Figure 3 indicates FE-SEM

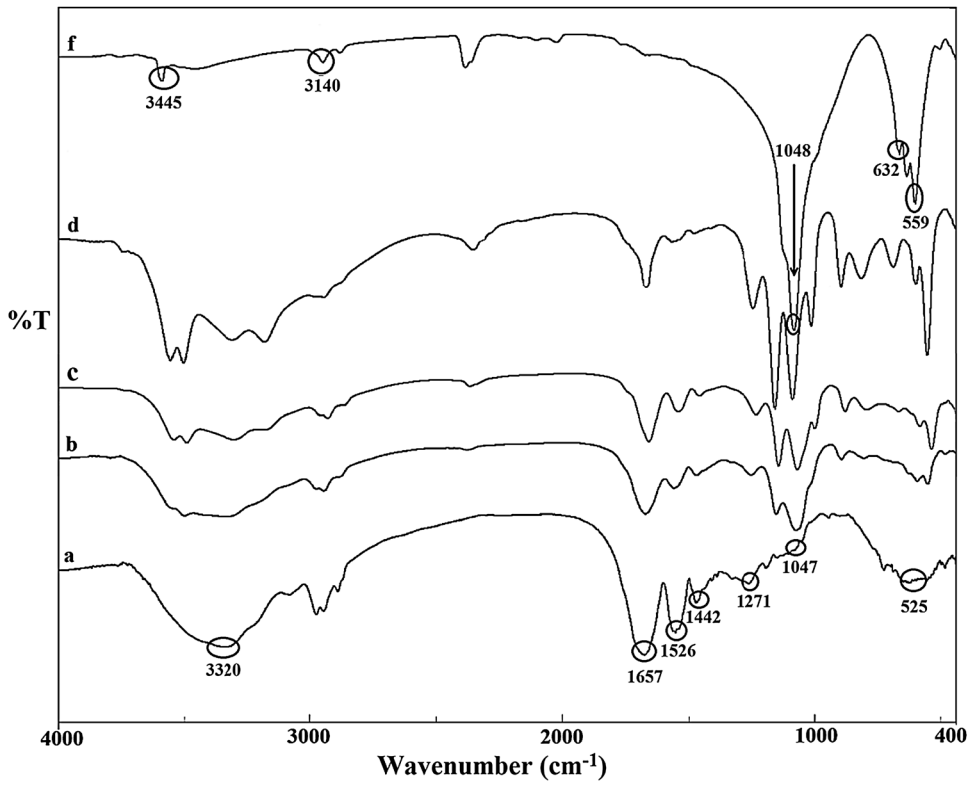

Fig. 2 FT-IR spectra of pure Zein (*a*), pure nHAp (*f*), and Zein/nHAp composite with different Zein content including 70 wt% (*b*), 50 wt% (*c*), and 30 wt% (*d*)

images of Zein/nHAp containing 30, 50, and 70 wt% nHAp, pure Zein, and pure nHAp. About composites, it is seen a porous structure with nanosized dimensions (< 100 nm) having high surface for appropriate adsorption of target dye. The nHAp content in composite influenced the intermediate porosity and the degree of interconnectivity. The increase in nHAp content led to a reduction in porosities owing to reaction junctions between nHAp and Zein [41]. Consequently, porosities of Zein/nHAp with different wt% of nHAp is in the order: 30 wt% nHAp > 50 wt% nHAp > 70 wt% nHAp.

Determination of specific surface area using N_2 adsorption/desorption measurements at 77 K expanded by Brunner–Emmett–Teller (BET) at equilibrium is applied to present helpful information on the adsorbent properties like surface area, total pore volume, and micropore area. 73.73 m^2/g, 0.249 cm^3/g, and 2.318 nm were acquired for surface area, total pore volume (V_p), and mean pore diameter, respectively. The BET and porosity values of Zein/nHAp were remarkably higher than that of pure Zein (0.1402 m^2/g) owing to the incorporation of nHAp resulting increase in the surface area of the adsorbent and consequently supplying more active sites and enhancement of adsorption efficiency. The nitrogen adsorption/desorption isotherm and the pore size distribution (inset) of Zein/nHAp composite are presented in Fig. 4.

The X-ray diffraction patterns of pure Zein (a), Zein/nHAp (e), and Zein/nHAp composite (b: 30 wt% nHAp, c: 50 wt% nHAp, d: 70 wt% nHAp) have been exhibited in Fig. 5. In Zein, a significant peak was observed at $2\theta = 20°$ (maximum intensity) corresponding to the characteristic peak of Zein showed that the polymer was amorphous [37]. In the composite, we observed both the Zein and n-HAp diffraction peaks. The peaks around $2\theta \approx 25.9°$, 31.8°, 32.2°, 32.9°, 34.1° and 39.8° relate to (002), (211), (112), (300), (202), (310) crystal faces of HAp, respectively [21]. In addition, the peaks of nanocomposite are slightly broader than pure HAp which can be a sign for reducing the HAp size and crystallinity in the presence of Zein matrix [42].

Effect of Ratios of nHAp to Zein of Nanocomposites on Removal of Congo Red

Figure 6 shows the influence of ratios of nHAp to Zein on the removal of CR. Removal percent of CR grows with increasing of nHAp to Zein from 70/30 to 30/70, so the optimum ratio is Zein/nHAp composite with ratio of 30/70. Also, the results showed that composite of Zein and nHAp have a synergistic effect on the removal of Congo red from aqueous solutions. In composite, Zein is a bed for nHAp and hydroxyapatite nanoparticles increase surface of Zein. The intermolecular hydrogen bonding between hydroxyl groups of nHAp and the oxygen of Zein can be expected.

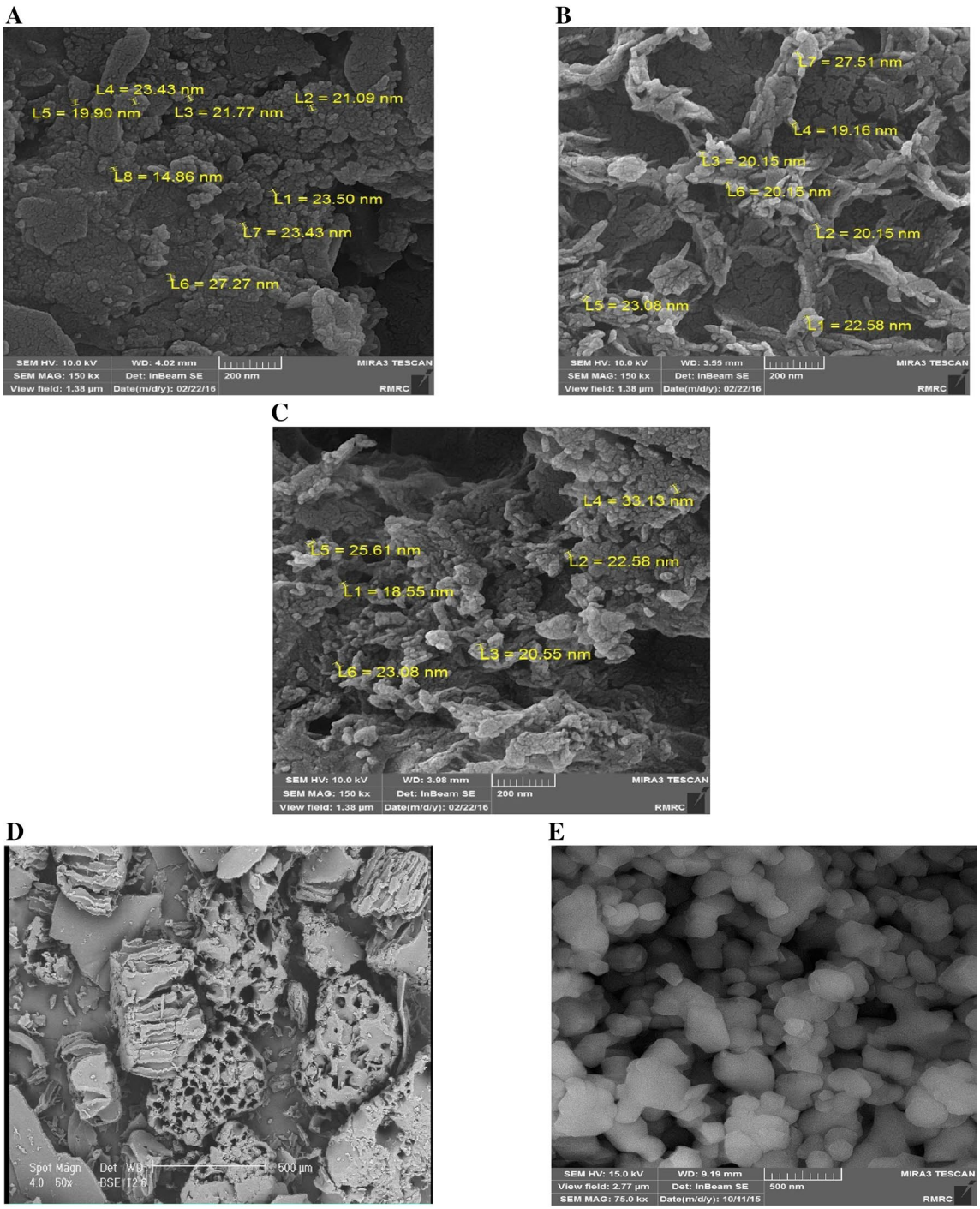

Fig. 3 FE-SEM images of Zein/nHAp consist of 30 (**a**), 50 (**b**), and 70 (**c**) wt% nHAp, and SEM images of pure Zein (**d**), and pure nHAp (**e**)

Central Composite Design

As it is obvious from CCD (Table 1) the influence of five independent variables such as pH, adsorbent dosage, CR concentration, contact time, and temperature were explored. Table 2 exhibits thirty-two experiments and their relating responses. Analysis of variance (ANOVA) was done for the removal percentage of the dye applying design expert 7.0.0 Trial (Table 3). The quality of the polynomial model equation was evaluated based on the coefficient of determination R^2 and statistical significance of the equation was assessed by F-test. P-values < 0.05 is a criterion for judgment about the significance of each term, and showed significant variables at 95% confidence level. Therefore, the following

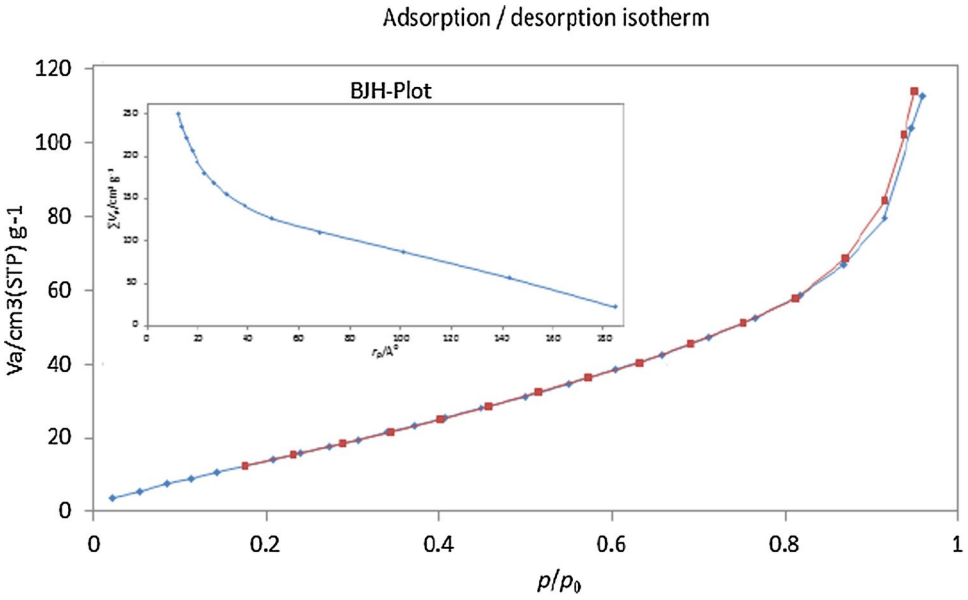

Fig. 4 N_2 adsorption–desorption isotherm and pore size distribution using BJH method (inset) of Zein/nHAp composite

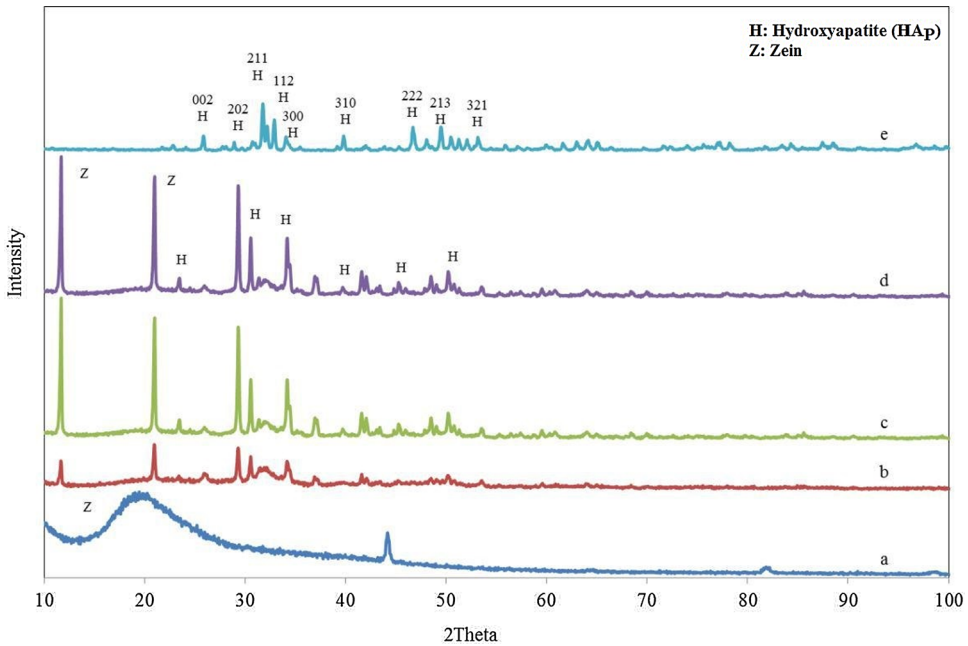

Fig. 5 XRD patterns of pure Zein (*a*), nHAp (*e*), and Zein/nHAp composite (*b* 30 wt% nHAp, *c* 50 wt% nHAp, *d* 70 wt% nHAp)

predictive models illustrating the removal percentage of CR dye was achieved in terms of important variables.

Equation (7) illustrates the relation between removal efficiency (R%) and the actual independent variables:

$$\begin{aligned} R\%_{(CR)} &= +102.45 + 2.00X_1 - 0.29X_2 - 0.21X_3 - 0.06X_4 \\ &\quad + 228.89\,X_5 + 4.44\text{E} - 003\,X_1X_2 + 0.016\,X_1X_3 \\ &\quad - 88.89\,X_1X_5 + 5.37\text{E} - 004\,X_2X_4 - 15.56\;X_2X_5 \\ &\quad + 3.89\text{E} - 004\,X_3X_4 + 2.22\,X_3X_5 + 2.28X_4X_5 \\ &\quad - 0.18\,X_1^2 + 2.46\text{E} - 003\,X_2^2 - 4.28\text{E} - 004\,X_3^2 \\ &\quad + 5.41\text{E} - 005\,X_4^2 + 179.57\,X_5^2 \end{aligned} \tag{7}$$

Figure 7a shows the correlation between experimental and predicted dye adsorption efficiency. It is seen there is a good fit between the experimental data and the predicted results. According to ANOVA for the $R\%_{(CR)}$, the P-value for the lack of fit was indicating the suitability of the predictive model. The closeness of the R^2 value to unify represents more accuracy of response predicted by the model. The R^2 value of 0.9959 and adjusted R^2 value of 0.9884 confirm the goodness of the fit, and the predicted R^2 of 0.9360 is in reasonable agreement with the adjusted R^2. Figure 7b shows the residual plot versus predicted data and the random pattern of residuals presents adequacy of the model. An

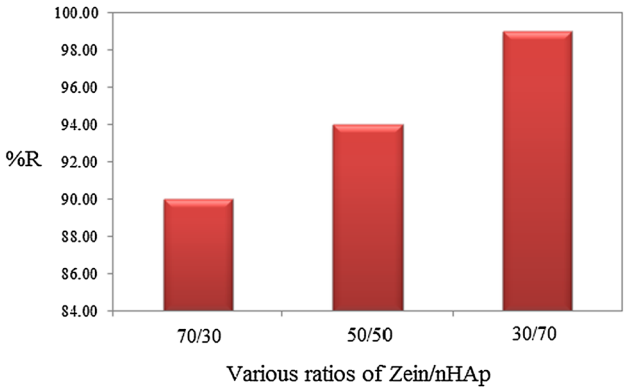

Fig. 6 Influence of various Zein/nHAp composite ratio on removal of CR. values are mean ± SD (n = 4) for CR. Concentration: 40 mgl^{-1}, adsorbent dosage 0.01 g, natural pH, temprature 25 °C and equilibrium time 30 min

adequate precision (signal-to-noise ratio) value higher than 4 is favorable. A value of 55.45 was discovered in the present work. Thus, this model can navigate the design space [43]. The coefficient of variation (C.V.%) denotes the degree of precision and reliability of the model [33]. The C.V. value of 0.10 confirms high precision and reliability of the experimental data (C.V.% < 10 indicates high reproducibility of experimental data) [34]. The normal distribution of data was discovered by plotting the residuals and deviations of the observed data amounts from the predicted amounts (Fig. 7c). Obviously, the figure expressed that the experimental data fall close enough to the straight line for CR adsorption suggesting the fair adequacy of the constructed equation for predicting the adsorption and evaluating individual interactions between the response and process variables.

Three-Dimentional Response Surface Plot

The 3D response surface plot is a three-dimensional graphic representation that was portrayed and regarded to

Table 3 ANOVA of the second-order polynomial equation for removal efficiency (%) of CR by Zein/nHAp nanocomposite

Source	SS[a]	df[b]	MS[c]	F value	P value	Remark
Model	25.91	20	1.30	133.53	< 0.0001	Highly significant
X_1	6.667E−003	1	6.667E−003	0.69	0.4247	Not significant
X_2	0.43	1	0.43	43.98	0.0001	Highly significant
X_3	0.28	1	0.28	29.04	0.0002	Highly significant
X_4	2.94	1	2.94	303.07	< 0.0001	Highly significant
X_5	0.13	1	0.13	13.92	0.0033	Significant
X_1X_2	0.040	1	0.040	4.12	0.0672	Not significant
X_1X_3	0.49	1	0.49	50.51	< 0.0001	Highly significant
X_1X_4	0.000	1	0.000	0.000	1.0000	Not significant
X_1X_5	1.44	1	1.44	148.44	< 0.0001	Highly significant
X_2X_3	0.56	1	0.56	57.98	< 0.0001	Highly significant
X_2X_4	2.10	1	2.10	216.73	< 0.0001	Highly significant
X_2X_5	1.10	1	1.10	113.65	< 0.0001	Highly significant
X_3X_4	1.10	1	1.10	113.65	< 0.0001	Highly significant
X_3X_5	0.023	1	0.023	2.32	0.1560	Not significant
X_4X_5	3.42	1	3.42	352.80	< 0.0001	Highly significant
X_1^2	4.67	1	4.67	481.61	< 0.0001	Highly significant
X_2^2	0.56	1	0.56	57.93	< 0.0001	Highly significant
X_3^2	0.017	1	0.017	1.75	0.2121	Not significant
X_4^2	5.64	1	5.64	581.18	< 0.0001	Highly significant
X_5^2	2.424E−005	1	2.424E−005	2.499E−003	0.9610	Not significant
Residual	0.11	11	9.701E−003			
Lack of Fit	0.064	6	0.011	1.23	0.4177	Not significant
Pure Error	0.043	5	8.600E−003			
Cor Total	26.01	31				

$R^2 = 0.9959$, Adj $R^2 = 0.9884$, Pred $R^2 = 0.9360$

[a]Sum of square

[b]Degree of freedom

[c]Mean square

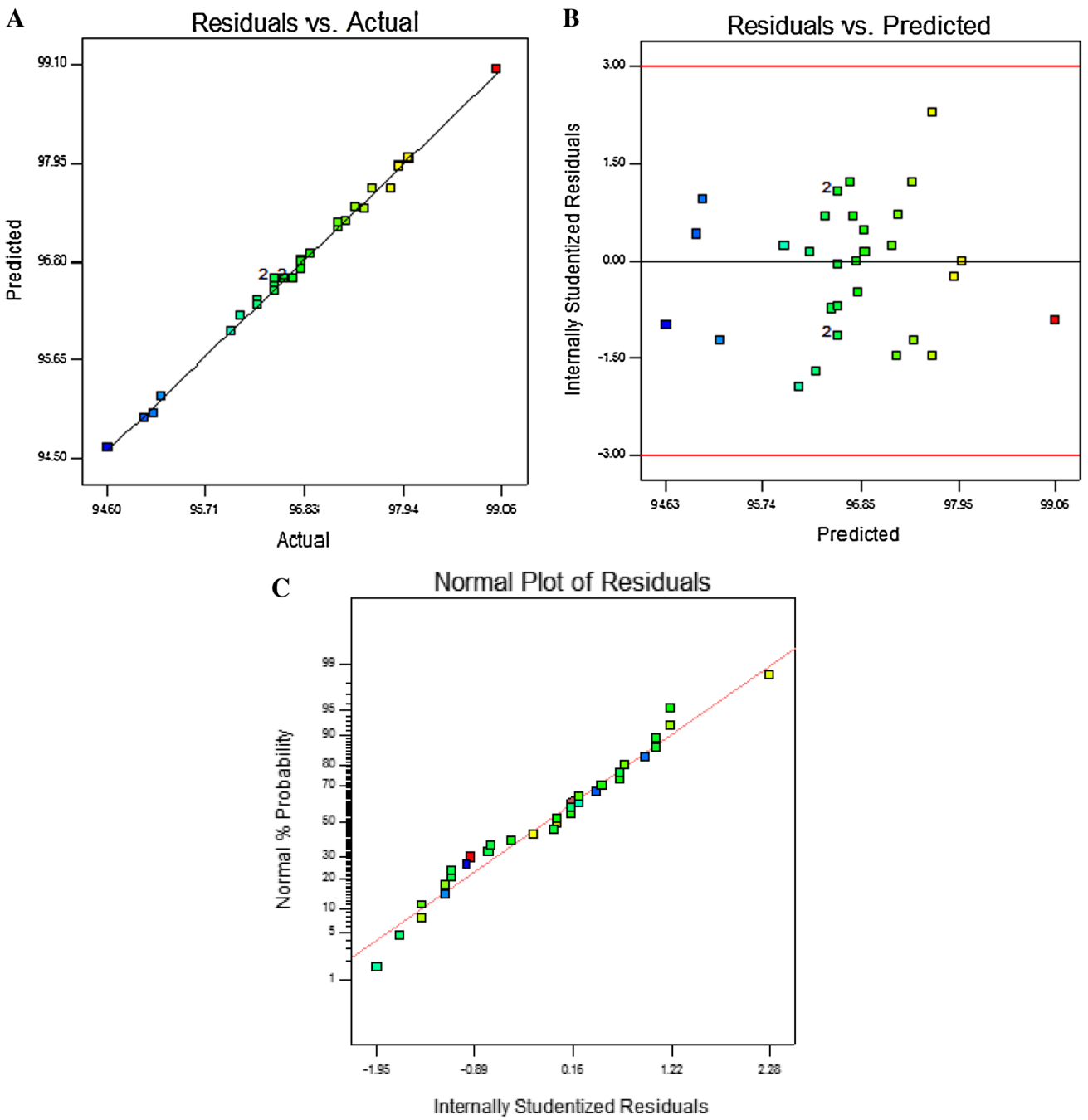

Fig. 7 **a** The experimental data versus predicted data, **b** the residuals versus predicted data, and **c** normal plot for removal of CR

optimize important factors such as pH, adsorbent dosage, CR concentration, contact time, and temperature as well as to provide helpful information about the possible interaction on variables [14]. The importance of the standard equation coefficients, the geometric nature of the surface, and the maximum and minimum of the response can be examined by the response surface. Figure 8 shows the most corresponded appropriate response surface for the design and indicates the response surface plots of R% (removal percentage of CR) variables.

The curvatures of these plots show the interaction between variables. The effect of pH on the adsorption capacity of the nanocomposite was studied in the range of 3–9. Based on Fig. 8a, as the pH increased, no significant change occurred in the removal percentage of CR. So the pH value of the solution is not an important monitoring parameter.

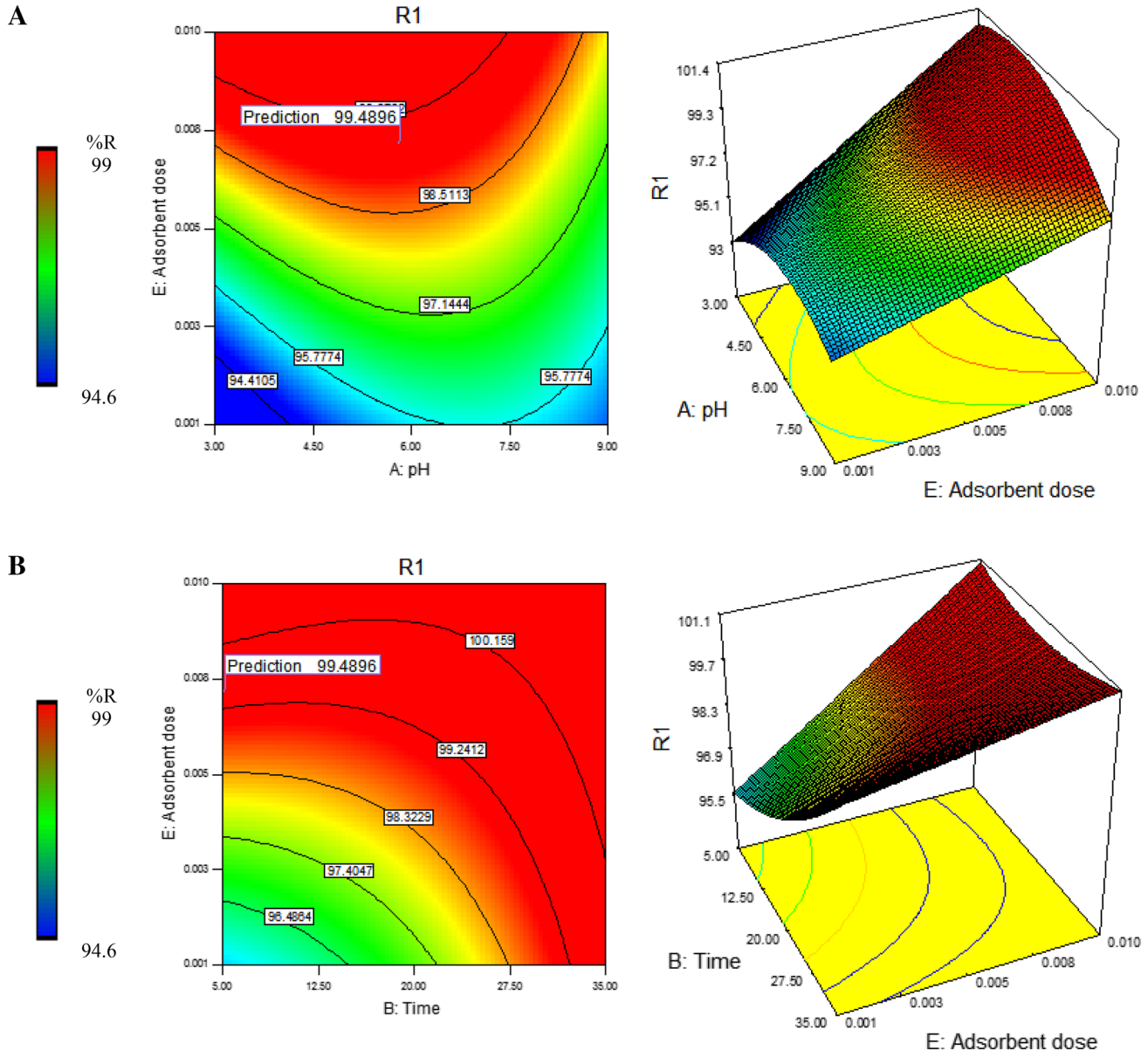

Fig. 8 The 3D response surface plots and contour plots for interactive effect of **a** pH and adsorbent dosage, **b** Time and adsorbent dosage, **c** Temprature and adsorbent dosage, and **d** CR concentration and adsorbent dosage

As mentioned in ANOVA table, pH is not a significant factor in the removal of CR by Zein/nHAp adsorbent. This is an advantage because this adsorbent can be applied in real samples in every pH with high removal percent of CR. The maximum removal percentage of 99.4896 was achieved at pH 5.83 which was considered as optimum pH. Seemly, at this area, the electrostatic attraction between negative charge of CR molecules and the positive charge of adsorbent is the main adsorption mechanism. Hydroxide competition with CR molecules for adsorption sites may be the reason of slight decrease in CR removal percentage at higher pH. Although it is thought that the electrostatic bond is not the only mechanism for adsorption. Because pH is not a significant factor in this study, as expressed earlier. In fact, due to the presence of Zein, dye molecules can be captured in pores of the adsorbent which is another reason.

Another factor that severely impresses the percentage of dye removal, is contact time because of reaching the equilibrium between aqueous solution and adsorption process. The influence of contact time on the adsorption efficiency of the nanocomposite was studied in the range of 5–35. As it is seen in Fig. 8b, in the first stage of a adsorption process, the removal efficiency is fast because of the high performance of adsorbent and achieving equilibrium. Therefore, the

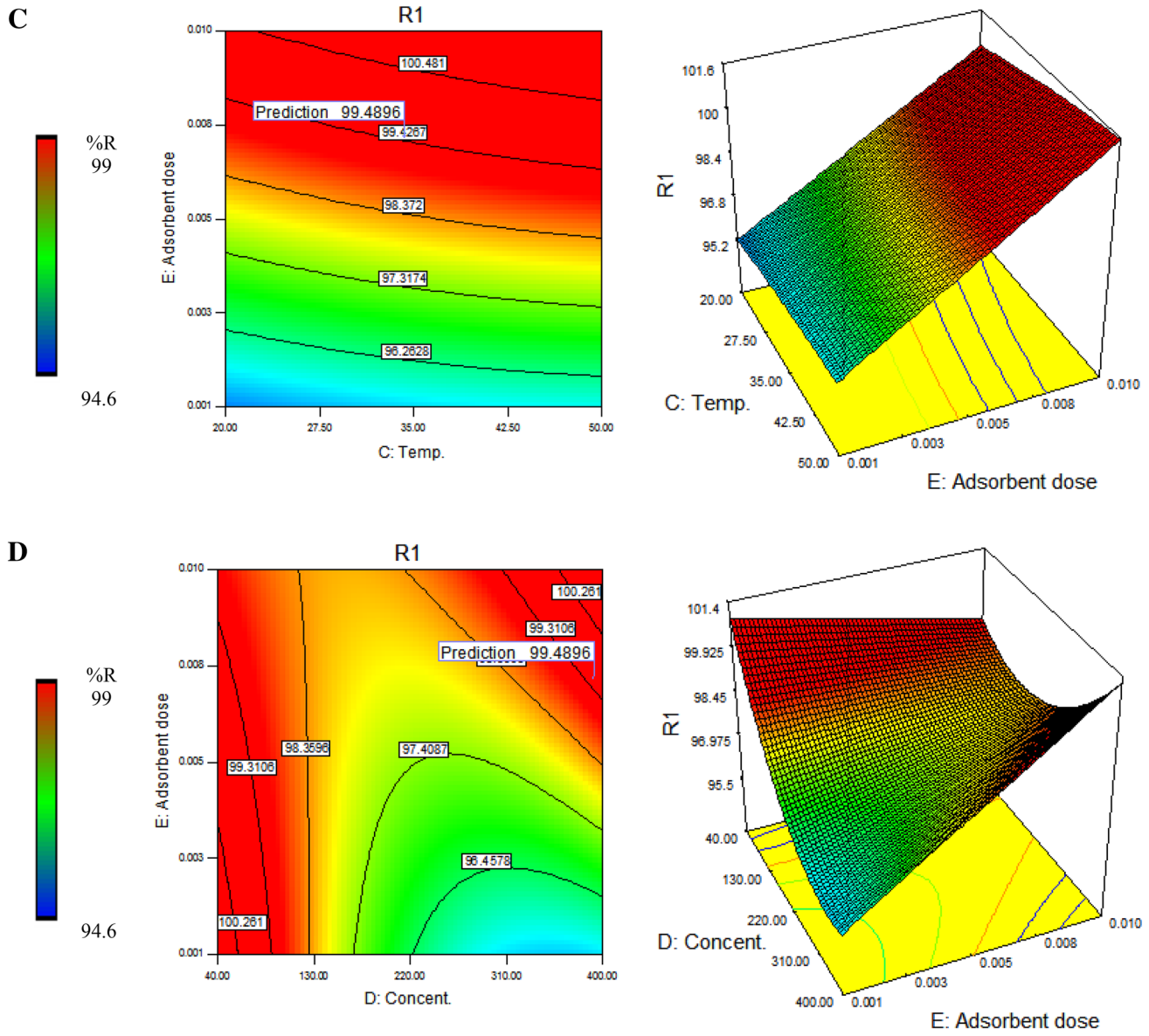

Fig. 8 (continued)

maximum adsorption performance was obtained within the first 5 min and consequently reached equilibrium at about of 5.20 min of contact time.

Temperature is one of the most important parameters in all separation procedures, particularly adsorption processes. The influence of temperature was investigated in the range of 20–50 °C and the maximum removal efficiency was achieved at 34.32 °C. As shown in Fig. 8c, CR adsorption improves with rising temperature. The increase in removal efficiency with rising temperature results from the movability of the dye molecules which enhances and leads to increment of CR adsorption on the surface of adsorbent.

The initial concentration presents a prominent driving force to overwhelm all mass transfer resistance of CR molecules between the aqueous and solid phases [44, 45]. The effect of initial concentration of CR on the removal efficiency was studied in the range of 40–400 ppm. Based on Fig. 8d, it was found adsorption rate enlarged at both low and high concentration of CR and the maximum removal efficieny was obtained at 392.10 ppm as optimum concentration of CR. At lower concentration of CR increase in removal percentage is due to abundance of vacant sites on the adsorbent surface to the dye which results in enhancement of CR diffusion rate to the sorbent. But at high concentration of CR the unoccupied sites of adsorbents become fewer and mass transfer is dependent on the initial dye concentration. In fact, increase in CR concentration reduces resistance to the adsorption of solute from CR solution and

accelerates the diffusion of CR from the solution onto the adsorbent owing to the growth of driving force (concentration gradients).

The influence of adsorbent dosage on the CR removal in the range of 0.001–0.010 g is shown in Fig. 8d. It can be seen by increasing the amount of adsorbent the amount of adsorbed CR remarkably enhanced and reached its maximum at 0.007 g (optimum adsorbent dosage). An increment in adsorption efficiency with enhancement of adsorbent dosage is illustrated by improvement of surface area and reactive sites to dye molecules as well as increasing in concentration gradient which leads to improvement of the rate of CR mass transfer to the adsorbent surface.

Optimization Process

In order to achieve the maximum removal efficiency of CR, RSM is applied to give the optimum combination of variables based on the ridge maximum analysis and the canonical analysis. The experiment with desirability value of 1 was chosen by utilizing the optimization function of the software. The desirability function is defined as:

$$D = (d_1 \times d_2 \times \ldots d_n)^{1/n} = \left(\prod_{i=1}^{n} d_i\right)^{1/n} \quad (8)$$

where n is the number of responses in the measure and d_i is the desirable ranges for each response.

The function of desirability was employed to confirm the model. The optimum amounts of regarded parameters were acquired by solving the regression equation and by studying the response surface contour and 3D plots. The changeability independent parameters was interpreted by the multiple coefficients of determination R^2. Also, the model equation was exerted to anticipate the optimum value and to clarify the interaction between the factors within the specified range [46, 47]. Optimal conditions of the tested parameters were set as follows in Table 4, and under the optimum conditions, the removal efficiency of 99.48% was obtained.

Modeling and Optimization by ANN-GA

An artificial neural network has been successfully exerted for prediction of adsorption data achieved at different experimental data [48]. The measures such as maximum value of

Table 4 Predicted and experimental value of responses at the optimum condition

Approach	Factors					Response	
	pH	Concentration (ppm)	Adsorbent dose (g)	Time (min)	Tempreture (°C)	Experimental	Predicted
CCD	5.83	392.10	0.007	5.20	34.32	99.50	99.48

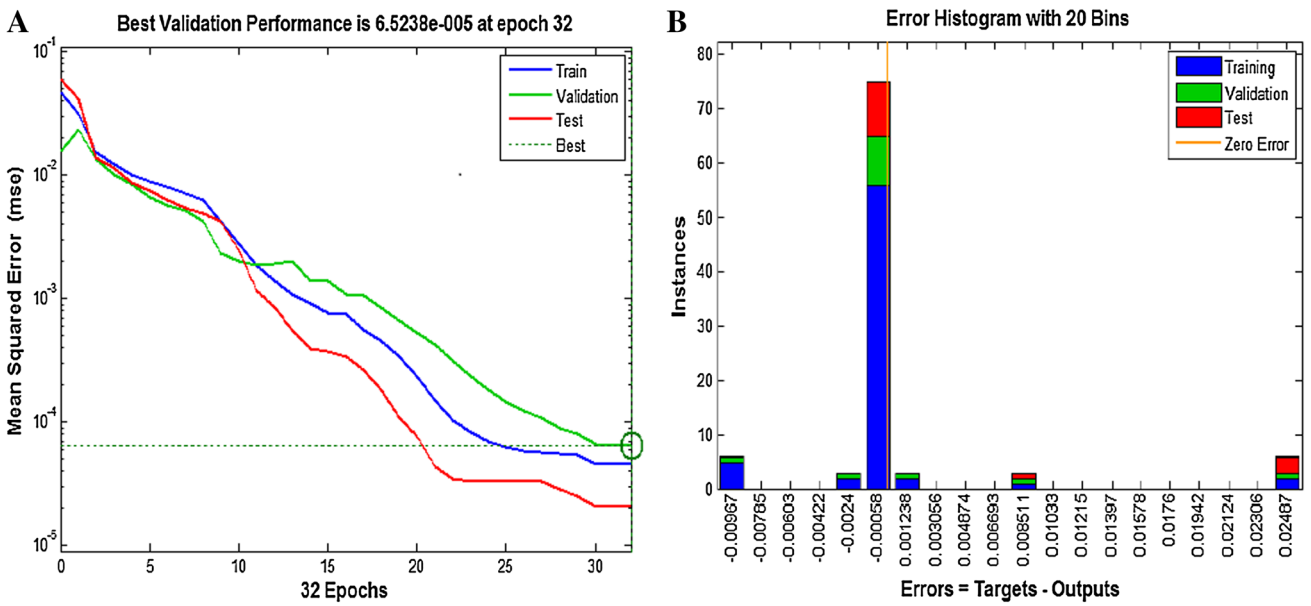

Fig. 9 **a** The training, validation and test performance (**b**), and the error histogram of the network

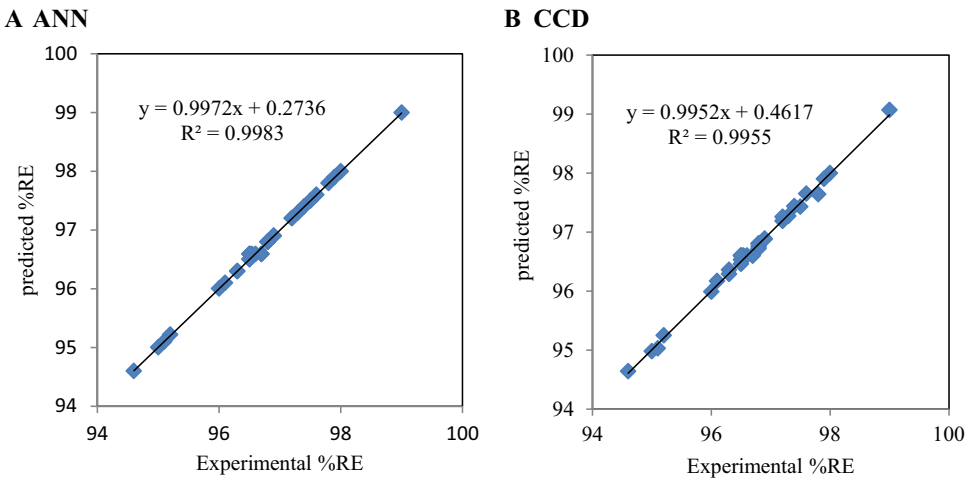

Fig. 10 The predicted %RE values by the ANN modeling (**a**) and CCD (**b**) versus the experimental %RE values

R^2 and the lowest value of MSE for testing set was taken into account for option of the optimum ANN structure. Figure 9a, b indicates the MSE versus the number of epochs for optimal ANN and Fig. 10a, b presents the predicted data versus actual response obtained from the CCD and ANN results.

The Fig. 10a, b demonstrated the goodness of fit between experimental data and predicted data given by ANN model in comparing with the CCD result. Lately, combination ANN-GA has been successfully employed aiming to the optimization of different systems. In this work, GA utilized by equations that obtained from ANN models. The method begins by using optimization variables such as pH, temperature, contact time, initial concentration of CR, and adsorbent dosage. The objective function was that equation obtained from ANN model which connect the inputs with output and can be defined as follows:

$$\left(ANN_{output}\right) Y = purelin\left(LW \times tansing(IW \times \left[x_1;x_2;x_3;x_4;x_5\right] + b_1\right) + b_2 \quad (9)$$

where (x_1), (x_2), (x_3), (x_4), and (x_5) symbolize the inputs, LW, IW, b_1 and b_2 are the weights and bias of hidden and output layers. Table 5 exibits the weight and bias values of each layer aquired from the best ANN model.

The Matlab genetic algorithm toolbox has been used for GA processes with generation, a population size of with scattered crossover function of based on rank scaling function and stochastic uniform option. Figure 11a, b population size of 20 with scattered crossover probability of 0.8 Rank scaling function and Stochastic uniform option. The maximum removal percentage of the dye at pH of 5.954, temperature of 29.435, contact time of 6.335 min, 0.007 mg of adsorbent, 357.33 ppm initial dye concentration was predicted by ANN-GA (Table 6). The optimum conditions acquired from ANN-GA hybrid and CCD (Table 6) experimental the efficiency of Congo red removal 99.50 that shows agreement between the two methods. The MAPE (%) of 0.0494 and 0.0155 were obtained for RSM (CCD) and ANN, respectively, also Fig. 12 shows the MAPE (%) of RSM (CCD) and ANN versus number of experiments. The MAPE and MSE values of ANN model are obviously least than CCD model for each experiment, so the accuracy of ANN model.

Table 5 The weight and bias of trained ANN for predicting the removal efficiency of the Congo red dye

IW				LW	b_1	b_2
1.5079	0.9968	−0.4682	−1.6931	−0.4600	−2.2162	−0.5221
−1.1009	0.8318	1.1397	−0.1792	1.1857	1.1915	
0.8792	−1.1088	−0.5413	0.2578	−0.1135	−2.1425	
−0.3703	0.7666	0.0185	2.4622	0.5176	−0.5961	
−0.5323	−1.5878	−2.0041	−2.0116	0.7473	−1.6887	
−1.1251	1.5454	1.3494	−1.2320	−0.3990	0.5438	
1.9261	−0.3241	1.0620	0.6562	1.1767	1.4568	
1.2194	−1.9855	−0.1579	1.5424	0.1780	2.4654	
0.3298	0.6818	−0.8556	−1.4359	1.1786	−2.3483	

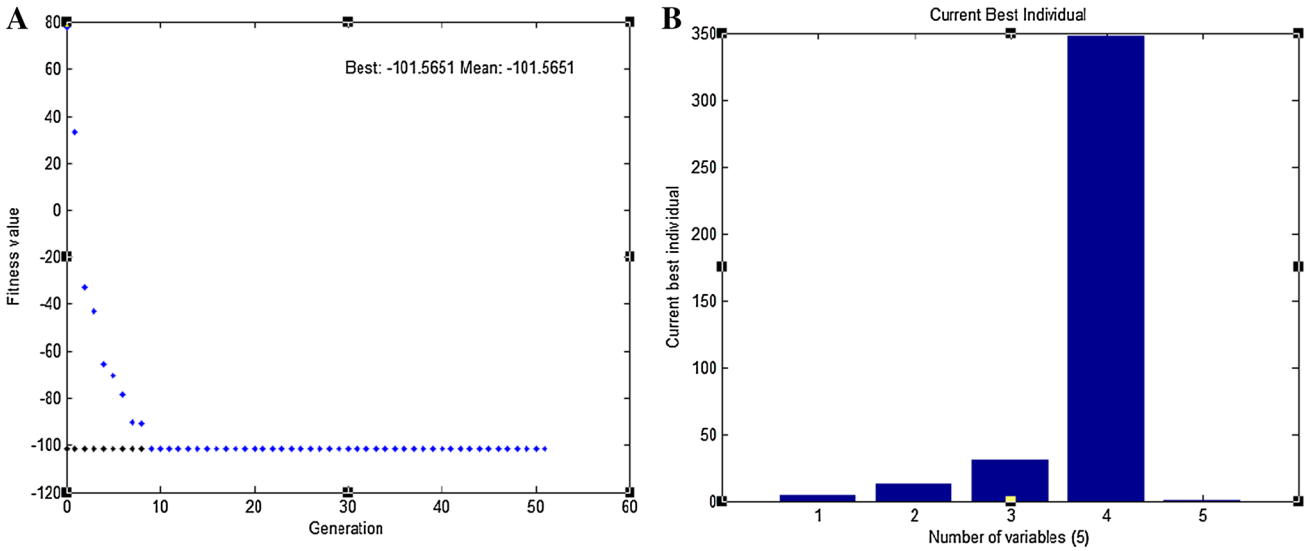

Fig. 11 Plots of best fitness and best individual for the removal efficiency of Congo red dye by ANN-GA method

Comparison of CCD and ANN-GA

The CCD and ANN-GA are two powerful prediction techniques able to solve linear and non-linear problems [49]. The CCD and ANN-GA were successfully used for adsorption of CR by Zein/nHAp. Both models were well fitted to experimental response.

Although, the main limitation of CCD is ability to solve only quadratic non-linear correlation but the ANN-GA is capable of solving any form of non-linearity [20, 50]. The suitability of CCD and ANN-GA in the suggested process was determined applying MAPE (%) values and the determination coefficients (R^2) of two models ware compared (computed based on Eq. 20) [51].

Where n is the number of points, y_i is the forecasted value, y_{di} is the experimental value, and y_m is the average of the experimental values 0.0155 and 0.0494 amounts of MAPE was discovered for CCD and ANN-GA respectively. According to Fig. 12 indicating the MAPE (%) of CCD and ANN-GA against number of experiments, the MAPE amount of CCD was found to be more than ANN-GA model for each experimental test which signifies higher accuracy of ANN-GA than CCD. R^2 is an expressive to present the prediction potential of the model for the process. 0.9955 and 0.9983 values of R^2 were achieved for CCD and ANN-GA respectively.

The presence of high degree of agreement between experimental data and forecasted data expresses that ANN-GA is more powerful and effective than CCD for prediction and optimization of the influences of independent parameters on the removal performance of CR dye from aqueous solution.

Adsorption Isotherm Study

Adsorption isotherms investigation is very significant to obtain information about properties and mechanism of adsorption. The adsorption isotherms point out the partition of adsorbate molecules between the liquid sample solution and solid sorbent in the adsorption process. In fact, the adsorption studies are ascribed to the chemistry of the adsorbate and adsorbent at a particular temperature. Hence, to appraise the adsorption isotherm of the suggested method, the popular isotherms such as Langmuir and Freundlich were investigated at various concentrations in the range of (40–400) ppm at optimum conditions. Formation of a monolayer adsorbate where there are no any interactions between the adsorbed molecules is hypothesis of the Langmuir isotherm model. According to this assumption, the linearized form of Langmuir isotherm model is as below [52]:

$$\frac{c_e}{q_e} = \frac{1}{k_L q_m} + \frac{c_e}{q_m} \tag{10}$$

where C_e is the equilibrium concentration of the dye solution (ppm), the q_m constant is the maximum adsorption capacity (mg/g), and K_L is Langmuir constant (l/mg). The plot of C_e/q_e versus C_e, leads to a straight line for CR. K_L and q_m were obtained from the intercept and slope of the plots. The desirability of CR adsorption onto Zein/nHAp composite is determined by a dimensionless constant called separation factor, R_L.

$$R_L = \frac{1}{1 + K_L C_0} \tag{11}$$

Table 6 The comparison between optimum conditions of CCD and ANN-GA models

Approach	Factors					Response	
	pH	Concentration (ppm)	Adsorbent dose (g)	Time (min)	Tempreture (°C)	Experimental	Predicted
CCD	5.830	392.100	0.007	5.200	34.320	99.50	99.4896
ANN-GA	5.954	357.330	0.007	6.335	29.435	99.62	101.5651

Appraisal of ANN and RSM models	R^2	MSE	RMS	MAPE%
CCD	0.9955	0.0037	0.0607	0.0494
ANN	0.9983	0.0014	0.0065	0.0155

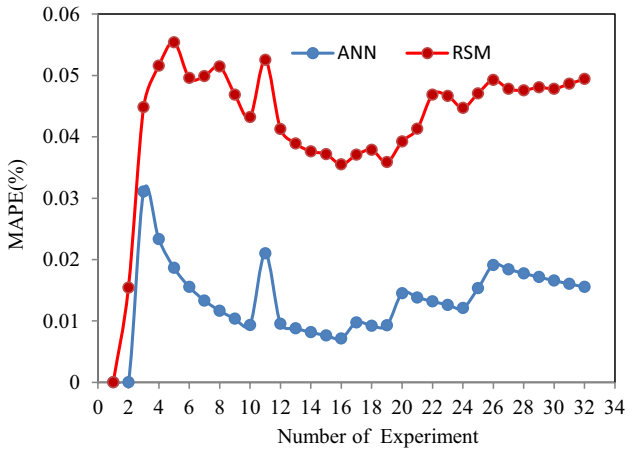

Fig. 12 MAPE (%) of RSM (CCD) and ANN versus number of experiments

Table 7 Isotherm constant parameters and correlation coefficients calculated for the biosorption of CR by nHAp/Zein nanocomposite

Model	Parameters	Value
Langmuir	q_{max} (mg g^{-1})	416.6600
	K_L (L mg^{-1})	0.1090
	R_L	0.02200
	R^2	0.9839
Freundlich	1/n	0.5583
	K_f (mg g^{-1})(L $mg^{-1})^{1/n}$	5.5533
	R^2	0.9681
Temkin	B_1	83.4460
	K_T (L mg^{-1})	1.3859
	R^2	0.9659
Dubinin-Radushkevic	q_m (mg g^{-1})	234.3230
	$\beta \times 10^{-7}$ (mol^2 J^{-2})	5.0000
	R^2	0.8190

where K_L is the Langmuir constant and C_0 (mg/l) is the initial concentration of the applied dye. The R_L value indicates the unfavorable ($R_L > 1$), linear ($R_L = 1$), favorable ($0 < R_L < 1$), and irreversible ($R_L = 0$) kind of adsorption process [53]. Based on the results given in Table 7, the value of R_L for CR dye is 0.022 which signifies the adsorption of Congo red on the Zein/nHAp adsorbent is favorable.

The Freundlich isotherm is widely used for many adsorption processes. In this work, the Freundlich isotherm was also studied for the process. The equation is as below:

$$q_e = k_f c_e^{\frac{1}{n}} \tag{12}$$

The linearized form of the Freundlich isotherm can be as following:

$$\ln qe = \ln K_F + \frac{1}{n} \ln Ce \tag{13}$$

where C_e, K_f, and 1/n are the equilibrium concentration of the dye (ppm), the Freundlich constant [(mg/g)(L/mg)$^{1/n}$], and heterogeneity factor that represents the adsorption intensity [52], respectively. The values of the constant 1/n and K_f were calculated from the slope and the intercept of the linear plot of $\ln q_e$ versus $\ln C_e$. The value of 1/n (0–1) shows the surface heterogeneity and the closer the value to zero the higher the heterogenity [52, 54–56]. As the results shown in Table 7, the value of 1/n was in the range of (0–1) which means the adsorption of CR dye of interest on the adsorbent was occured on a heterogeneous surface.

The heat of the adsorption and the adsorbent-adsorbate interaction were assessed applying Temkin isotherm model. The equation of this model is defined as follows [57]:

$$q_e = B_1 \ln K_T + B_1 \ln C_e \tag{14}$$

where B = (RT)/b (the constant B refers to the heat of adsorption), T is the absolute temperature (Kelvin), R is the universal gas constant (8.314 J/mol K). K_T is the equilibrium binding constant (L/mol) related to the maximum binding energy. B_1 and K_T constants were calculated from the slope and intercept of a linear plot of q_e against $\ln C_e$. Suitability of this model for fitting and well presentation of the experimental data related to the adsorption of CR on the adsorbent was proved by this model. Values obtained from the equation are exhibited in Table 7.

Dubinin–Radushkevich (D–R) isotherm model was chosen to an understanding of adsorption mechanism and to describe adsorption on both homogenous and heterogeneous surfaces [31]. A linear form of D–R isotherm is:

$$\ln q_e = \ln q_m - \beta\varepsilon^2 \tag{15}$$

$$\varepsilon = RTln\left(1 + \frac{1}{C_e}\right) \tag{16}$$

$$E = \frac{1}{\sqrt{2\beta}} \tag{17}$$

where q_m is the theoretical saturation capacity (mg g^{-1}), β, a constant of Dubinin-Radushkevich (mol^2 J^{-2}); ε, the Polanyi potential; E, related to free energy (kJ mol^{-1}); R, 8.314 gas constant (J mol^{-1} K^{-1}) and T, 273.15 absolute temperature (K).

Adsorption Kinetics

The adsorption kinetic modeling was carried out utilizing pseudo-first-order and pseudo-second-order models. These initial empirical models have been vastly applied to depict the kinetics of adsorption. The kinetic of CR adsorption on the Zein/nHAp was studied in relation to the pseudo-first-order (Eq. 18) and pseudo-second-order (Eq. 19) models [58], respectively.

$$\log(q_e - q_t) = \log(q_e) - \frac{K_1}{2.303}t \tag{18}$$

$$\left(\frac{t}{q_t}\right) = \frac{1}{K_2\, q_e^2} + \frac{1}{q_e}(t) \tag{19}$$

where q_e and q_t exhibit the precise value of the adsorbed dye at equilibrium and every time (mg/g), K_1 (1/min) and K_2 (g/mg min) are the adsorption rate constant. K_1 and K_2 are calculated by the slopes of both lines, while the intercept of lines are used to compute experimental adsorption capacity [59, 60].

The intraparticle diffusion equation is expressed as [31]:

$$q_t = k_{dif} t^{1/2} + C \tag{20}$$

where K_{dif} is the intraparticle diffusion rate constant (mg/(g min$^{1/2}$)) and C indicates the boundary layer thickness.

The linear form of Elovich model is generally given as [31]:

$$q_t = \frac{1}{\beta}\ln(\alpha\boldsymbol{\beta}) + \frac{1}{\beta}\ln(t) \tag{21}$$

The experimental results given in Table 8, indicate the closeness of theoretical and experimental adsorption capacity for pseudo-second-order kinetic model that approved by the higher value of correlation coefficient over whole adsorption step which means the suitability of this model for studying experimental data.

Thermodynamic Study

The change in some thermodynamic parameters such as free energy ($\Delta G°$), entropy ($\Delta S°$), and enthalpy ($\Delta H°$) were determined using equations below [20]:

Table 8 Kinetic parameters for the biosorption of CR by Zein/nHAp nanocomposite

Model	Parameters	Value
Pseudo-first-order	k_1 (min^{-1})	0.8558
	q_e(calc) (mg g^{-1})	38.8955
	R^2	0.6514
Pseudo-second-order	k_2 (g mg^{-1} min^{-1})	0.0040
	q_e(calc) (mg g^{-1})	476.19
	R^2	0.9985
Intraparticle diffusion	k_{dif} (mg g^{-1} min$^{-1/2}$)	77.793
	C	252.03
	R^2	0.9706
Elovich	β (mg g^{-1} min^{-1})	0.0157
	α (g mg^{-1})	52,458
	R^2	0.9817
	qe (exp) (mg g^{-1})	445.87

Table 9 Thermodynamic parameters for the biosorption of CR by Zein/nHAp nanocomposite in concentration of 400 mg l^{-1}

T (K)	lnK_e	ΔG° (KJ mol^{-1})	ΔH° (KJ mol^{-1})	ΔS° (KJ mol^{-1} K^{-1})	R^2
283.15	18.6421	−6.88676	4.1862	0.0094	0.9807
293.15	17.1428	−6.92564			
303.15	15.9179	−6.97505			
313.15	15.4609	−7.12928			
323.15	14.8258	−7.24426			
333.15	14.1122	−7.3318			

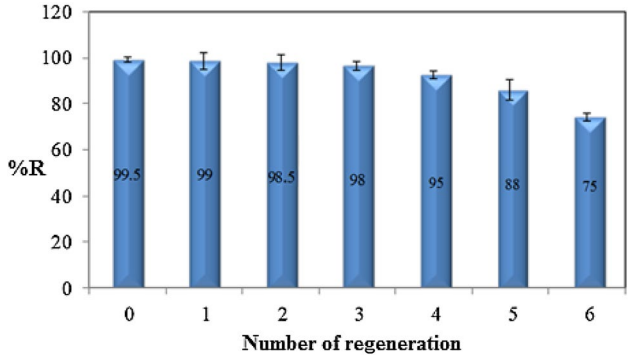

Fig. 13 Regenerate of Zein/nHAp nanocomposite of CR dye by pure ethanol solvent. Values are mean ± SD (n = 4)

Table 10 Removal percentages of CR from industrial wastewaters using Zein/nHAp adsorbent developed in this work ($N = 4$)

Sample	CR (mg/l)	% Removal
Industrial wastewaters	40	97 ± 1.89
	80	94 ± 2.36
	120	90 ± 2.58

$$lnK_{eq} = \frac{\Delta H^{\circ}}{RT} + \frac{\Delta S^{\circ}}{R} \tag{22}$$

$$K_{eq} = \frac{q_e}{C_e} \tag{23}$$

$$\Delta G^{\circ} = -RTlnK_{eq} \tag{24}$$

$$\Delta G^{\circ} = \Delta H^{\circ} - \mathrm{T}\Delta S^{\circ} \tag{25}$$

where C_e (mg/l), q_e (mg/g), R (J/mol k), T (k), and k_e (l/g) are the equilibrium concentration of CR dye in solution, the value of CR adsorbed onto adsorbent, the gas constant, absolute temperature, and the adsorption equilibrium constant, respectively. ΔH° and ΔS° are evaluated from the slope and intercept of plot of lnK_{eq} against 1/T. ΔG° can also be determined from true amounts of ΔH° and ΔS°. According to obtained results shown in Table 9, negative amount of ΔG° shows the adsorption process is thermodynamically spontaneous in nature [61]. The endothermic nature of adsorption process was approved by the positive amounts of ΔH°. In addition, the positive value of ΔS° mmentions a increase in the randomness at the adsorbent and adsorbate solution interface over the adsorption process.

Recyclability of the Adsorbent

The recyclability of the sorbent is one of the most important parameters indicating the potential of the adsorption process. For this purpose, several eluents including acetone, pure methanol, pure ethanol and mixture ethanol and methanol (1:1, v/v) were chosen to desorb of CR dye. In optimized condition, the maximum desorption was obtained in pure ethanol. Figure 13 indicates the regenerated Zein/nHAp nanocomposite that has high removal efficiency after six cycles.

Removal Performance of Zein/nHAp in Real Sample

To study Zein/nHAp adsorbent efficiency in a real sample, the sorption experiments were performed with industrial wastewater spiked with CR which are fed with different quantities of the dye. The results have been presented in Table 10. For this purpose, various amounts of CR (40, 80 and 120 mg/l) were spiked to the sample. Then, spiked samples were treated under the general procedure. The results demonstrate acceptable and excellent removal percentage confirming the good performance of adsorbent proposed for real sample.

Comparison with Other Adsorbents for Congo Red

Numerous adsorbents have been reported to apply for removal of CR. Table 11 compares the performance of different adsorbents for removal of CR. Based on obtained results, the performance of Zein/nHAp is superior to some other reported adsorbents in terms of higher adsorption capacity of the adsorbent.

Table 11 Performance of some different adsorbents for removal of CR

Adsorbent	pH	Adsorbent dose (g)	Concentration (mg/l)	Contact time (min)	q_m	References
Palladium nanoparticles loaded on activated carbon (Pd NPs-AC)	6	0.025	n.a	24	76.92	[62]
Silver nanoparticles loaded on activated carbon (Ag-NPs-AC)	4–7	0.025	n.a	14	66.67	[62]
Zinc oxide nanorods loaded on activated carbon (ZnO-NP-AC)	7	0.025	n.a	7	142.86	[62]
Activated carbon-Myrtus communis (AC-MC)	6	10	30	90	10	[63]
Activated carbon-Pomegranante (AC-PG)	7	20	30	90	19.23	[63]
Multiwalled carbon nanotube (MWCNT)	1	0.022	6	< 12	357.14	[64]
Nickel doped Zinc Sulfide nanoparticle loaded on activated carbon (Ni-ZnS-NP-AC)	3	0.03	10	22	285.7	[5]
Palladium nanoparticles loaded on activated carbon (Pd-NP-AC)	2	0.04	10	26	126.6	[5]
Fly ash	10.2	6.5	100	10	4.125	[65]
Banana peel	7.9	1	100	n.a	18.20	[66]
Neem leaf powder (NLP)	4, 6	0.6	40	300	72.40	[67]
Fertilizer plant waste carbon (WC)	7	1	20	300	233..9	[68]
Hierarchical porous zinc oxide (ZnO)	n.a	0.5	50	180	334	[69]
Zein-Nanohydroxyapatite (Zein/nHAp)	5.83	0.007	392.10	5.20	416.66	Present work

Conclusion

In this study, the Zein/nHAp, as an effective sorbent, was successfully prepared and characterized by FT-IR, FE-SEM, XRD, and BET in order to be applied for removal of CR dye from aqueous solution. The optimum conditions for pH, temperature, time, initial concentration of the dye, and sorbent dosage were discovered to be 5.83, 34.32 °C, 5.20 min, 392.10 ppm, and 0.007 g, respectively. The maximum removal efficiency of 99.49% was obtained experimentally under optimum conditions confirming the high adsorption ability of the adsorbent. The CCD and ANN-GA, as statistical models, were used to optimize significant parameters with MAPE (%) of 0.0494 and 0.0155 and the determination coefficient of R^2 values of 0.9955 and 0.9983 respectively. Based on results, the best optimization of experimental data was acquired from the ANN-GA method. The equilibrium and kinetic models were investigated to study adsorption process. Adsorption of CR onto the adsorbent obeyed Langmuir model. The process kinetics were well fitted with Pseudo-second-order model. Thermodynamic studies proved that the adsorption process was spontaneous and endothermic in nature. A regeneration study of the material was also performed and it was discovered that the Zein/nHAp could be regenerated applying a solution of pure ethanol and reutilized with high performance. The data and methodology given in this article would be practical for designing the adsorbent for the removal of actual effluent. Besides, the results of this report motivate researchers to expand advanced and optimized systems, according to adsorption for the impressive treatment of wastewater.

Acknowledgements The authors appreciate Shahrekord University and the Center of Excellence for Mathematics, Shahrekord University. The authors also wish to thank Mehdi Javaheran Yazd for his assistance in various stages of the work.

References

1. You H, Chen J, Yang C, Xu L (2016) Colloids Surf A 509:91–98
2. Yagub MT, Sen TK, Afroze S, Ang HM (2014) Adv Colloid Interface Sci 209:172–184
3. Ghaedi M, Daneshfar A, Ahmadi A, Momeni M (2015) J Ind Eng Chem 21:587–598
4. Haldorai Y, Shim J-J (2014) Appl Surf Sci 292:447–553
5. Ahmadi K, Ghaedi M, Ansari A (2015) Spectrochim Acta A Mol Biomol Spectrosc 136:1441–1449
6. Hou H, Zhou R, Wu P, Wu L (2012) Chem Eng J 211:336–442
7. Sharma V, Rekha P, Mohanty P (2016) J Mol Liq 222:1091–1100
8. Li C, Cui J, Wang F, Peng W, He Y (2016) Desalination Water Treat 57(30):14060–14066
9. Konicki W, Hełminiak A, Arabczyk W, Mijowska E (2017) J Colloid Interface Sci 497:155–164
10. Qiu J, Feng Y, Zhang X, Jia M, Yao J (2017) J Colloid Interface Sci 499:151–158
11. Tian Y, Ju B, Zhang S, Hou L (2016) Carbohydr Polym 136:1209–1217
12. Serpone N, Horikoshi S, Emeline AV (2010) J Photochem Photobiol C 11(2):114–131
13. Vidal J, Villegas L, Peralta-Hernández JM, Salazar González R (2016) J Environ Sci Health A 51(4):289–296
14. Asfaram A, Ghaedi M, Hajati S, Rezaeinejad M, Goudarzi A, Purkait MK (2015) J Taiwan Inst Chem Eng 53:80–91
15. El-Bindary AA, El-Sonbati AZ, Al-Sarawy AA, Mohamed KS, Farid MA (2015) Spectrochim Acta A Mol Biomol Spectrosc 136:1842–1849
16. Li X, Qi Y, Li Y, Zhang Y, He X, Wang Y (2013) Bioresour Technol 142:611–619
17. Karimi H, Ghaedi M (2014) J Ind Eng Chem 20(4):2471–2476

18. Xu H, Zhang Y, Jiang Q, Reddy N, Yang Y (2013) J Environ Manag 125:33–40
19. Wei W, Sun R, Jin Z, Cui J, Wei Z (2014) Appl Surf Sci 292:1020–1029
20. Mohammadzadeh A, Ramezani M, Ghaedi A (2016) J Taiwan Inst Chem Eng 59:275–284
21. Yang L, Wei Z, Zhong W, Cui J, Wei W (2016) Colloids Surf A 490:9–21
22. Mehrabi F, Vafaei A, Ghaedi M, Ghaedi AM, Dil EA, Asfaram A (2016) Ultrason Sonochem 38:672–680
23. Witek-Krowiak A, Chojnacka K, Podstawczyk D, Dawiec A, Pokomeda K (2014) Bioresour Technol 160:150–160
24. Dil EA, Ghaedi M, Asfaram A, Mehrabi F, Bazrafshan AA, Ghaedi AM (2016) Ultrason Sonochem 33:129–140
25. Rajendra M, Jena PC, Raheman H (2009) Fuel 88(5):868–875
26. Teimouri A, Ghanavati Nasab S, Vahdatpoor N, Habibollahi S, Salavati H, Chermahini AN (2016) Int J Biol Macromol 93:254–266
27. Teimouri A, Ghanavati Nasab S, Habibollahi S, Fazel-Najafabadi M, Chermahini AN (2015) RSC Adv 5(9):6771–6781
28. Gao X-Z, Liu H-J, Cheng F, Chen Y (2016) Chem Eng J 283:682–691
29. Dil EA, Ghaedi M, Ghaedi A, Asfaram A, Jamshidi M, Purkait MK (2016) J Taiwan Inst Chem Eng 59:210–220
30. Asfaram A, Ghaedi M, Goudarzi A, Rajabi M (2015) Dalton Trans 44(33):14707–14723
31. Ghaedi M, Khafri HZ, Asfaram A, Goudarzi A (2016) Spectrochim Acta A Mol Biomol Spectrosc 152:233–240
32. Ghaedi M, Ansari A, Bahari F, Ghaedi A, Vafaei A (2015) Spectrochim Acta A Mol Biomol Spectrosc 137:1004–1015
33. Asfaram A, Ghaedi M, Azqhandi MA, Goudarzi A, Dastkhoon M (2016) RSC Adv 6(46):40502–40516
34. Azad FN, Ghaedi M, Asfaram A, Jamshidi A, Hassani G, Goudarzi A et al (2016) RSC Adv 6(24):19768–19779
35. Dil EA, Ghaedi M, Ghaedi AM, Asfaram A, Goudarzi A, Hajati S et al (2016) J Ind Eng Chem 34:186–197
36. Ahmadizar F, Soltanian K, AkhlaghianTab F, Tsoulos I (2015) Eng Appl Artif Intell 39:1–13
37. Escamilla-García M, Calderon-Dominguez G, Chanona-Perez JJ, Farrera-Rebollo RR, Andraca-Adame JA, Arzate-Vazquez I et al (2013) Int J Biol Macromol 61:196–203
38. Yao C, Li Y, Wu F (2013) Polym Compos 34(7):1163–1171
39. Rajiv Gandhi M, Kousalya GN, Meenakshi S (2011) Int J Biol Macromol 48(1):119–124
40. Kumar PS, Srinivasan S, Lakshmanan V-K, Tamura H, Nair S, Jayakumar R (2011) Carbohydr Polym 85(3):584–591
41. Teimouri A, Azadi M (2016) Int J Polym Mater Polym Biomater 65(18):917–927
42. He J, Wang D, Cui S (2012) Polym Bull 68(6):1765–1776
43. Asfaram A, Ghaedi M, Hajati S, Goudarzi A (2015) RSC Adv 5(88):72300–72320
44. Çolak F, Atar N, Olgun A (2009) Chem Eng J 150(1):122–130
45. Dönmez G, Aksu Z (2002) Process Biochem 38(5):751–762
46. Somayajula A, Asaithambi P, Susree M, Matheswaran M (2012) Ultrason Sonochem 19(4):803–811
47. Ong S-T, Khoo E-C, Keng P-S, Hii S-L, Lee S-L, Hung Y-T et al (2011) Desalination Water Treat 25(1–3):310–318
48. Aber S, Daneshvar N, Soroureddin SM, Chabok A, Asadpour-Zeynali K (2007) Desalination 211(1–3):87–95
49. Khayet M, Cojocaru C, Essalhi M (2011) J Membr Sci 368(1):202–214
50. Sarve A, Sonawane SS, Varma MN (2015) Ultrason Sonochem 26:218–228
51. Bingöl D, Hercan M, Elevli S, Kılıç E (2012) Bioresour Technol 112:111–115
52. Muthukumaran C, Sivakumar VM, Thirumarimurugan M (2016) J Taiwan Inst Chem Eng 63:354–362
53. Nassar MY, Ahmed IS, Mohamed TY, Khatab MA (2016) RSC Adv 6(24):20001–20013
54. Foo K, Hameed B (2010) Chem Eng J 156(1):2–10
55. Agarwal S, Tyagi I, Gupta VK, Golbaz F, Golikand AN, Moradi O (2016) J Mol Liq 218:494–498
56. Munagapati VS, Kim D-S (2016) J Mol Liq 220:540–548
57. Kim Y, Kim C, Choi I, Rengaraj S, Yi J (2004) Environ Sci Technol 38(3):924–931
58. Labidi A, Salaberria AM, Fernandes SC, Labidi J, Abderrabba M (2016) J Taiwan Inst Chem Eng 65:140–148
59. Wu F-C, Tseng R-L, Juang R-S (2001) Water Res 35(3):613–618
60. Ho Y-S, McKay G (1999) Pseudo-second order model for sorption processes. Process Biochem 34(5):451–465
61. Sartape AS, Mandhare AM, Jadhav VV, Raut PD, Anuse MA, Kolekar SS (2013) Arab J Chem 10:S3229–S3238
62. Ghaedi M, Biyareh MN, Kokhdan SN, Shamsaldini S, Sahraei R, Daneshfar A et al (2012) Mater Sci Eng 32(4):725–734
63. Ghaedi M, Tavallali H, Sharifi M, Kokhdan SN, Asghari A (2012) Spectrochim Acta A Mol Biomol Spectrosc 86:107–114
64. Sheibani M, Ghaedi M, Marahel F, Ansari A (2015) Desalination Water Treat 53(3):844–852
65. Rao VB, Rao SRM (2006) Chem Eng J 116(1):77–84
66. Annadurai G, Juang R-S, Lee D-J (2002) J Hazard Mater 92(3):263–274
67. Bhattacharyya KG, Sharma A (2004) J Environ Manag 71(3):217–229
68. Mall I, Srivastava V, Kumar G, Mishra I (2006) Colloids Surf A 278(1):175–187
69. Lei C, Pi M, Jiang C, Cheng B, Yu J (2017) J Colloid Interface Sci 490:242–251